A1513

Towards model-based optimization of CGO/Ni anodes

Philip Marmet (1), Thomas Hocker (1), Jan G. Grolig (2), Holger Bausinger (2), Andreas Mai (2), Joseph M. Brader (3), Lorenz Holzer (1)
(1) Zurich University of Applied Sciences, Institute of Computational Physics
8401 Winterthur/Switzerland
(2) Hexis AG
8404 Winterthur/Switzerland
(3) University of Fribourg, Department of Physics
1700 Fribourg/Switzerland

Contact authors: www.EFCF.com/ContactRequest

Abstract

Gadolinium doped Ceria (CGO) is a promising material for SOFC anodes because of its mixed ionic electronic conductivity, its high catalytic activity for the hydrogen oxidation reaction (HOR) and its robustness against degradation. In SOFC research, electrochemical impedance spectroscopy (EIS) is an essential characterization tool, which serves as a basis for materials optimization on the electrode, cell and stack levels. However, for CGO based electrodes, there is no consensus how to interpret the impedance spectra yet. In the literature, especially the low frequency arc is often either depicted as gas impedance or as chemical capacitance process, without conclusive evidence. Further uncertainties in the interpretation of impedance spectra arise with respect to the operating conditions (especially pO_2, pH_2O) and to their impact on the HOR resistance. Hence, reliable interpretation of impedance spectra for SOFC with CGO-based anodes requires a detailed model, which captures a) the relevant physico-chemical processes, b) the associated material laws and c) the dependencies on varying operating conditions.
In the present contribution, we present an approach for a systematic materials optimization for CGO-based anodes, including EIS measurements, microstructure analysis and finite element modelling with AC and DC mode. The model captures all previously mentioned effects and their impact on the performance of a CGO/Ni-based anode. The computational model is validated and calibrated with EIS-measurements and the impacts of the chemical capacitance and gas impedance on the EIS spectra are illustrated for button cell conditions. The calibrated model is exemplarily used to optimize the CGO/Ni layer thickness. DC results of the extension of the reaction zone are thereby used to understand the different resistive contributions (e.g. from electrochemical conversion, from transport of charge carriers or from gas diffusion) to the total anode impedance.
In summary, we present a model-based approach to link bulk material properties, fabrication parameters, microstructure effects and operating conditions with the cell performance on button cell level. Moreover, the model can be extended to different scales like thin film electrodes, used for fundamental material characterization, as well as to large area cells used for industrial devices with stack architecture. By using a stochastic model for virtual structure variation, also the influence of the microstructure can be assessed in a fully digital way (digital materials design). Hence, with the integration of detailed physico-chemical properties over different scales into a single model framework, findings from basic and applied research can be directly used for the industrial development, enabling a systematic optimization of SOFC devices.

https://doi.org/10.5281/zenodo.4556899

1. Introduction

SOFC technology is a promising solution for the efficient use of renewable fuels or natural gas for heat and power. Thereby, doped Ceria represents an excellent material for SOFC anodes because of its mixed ionic electronic conductivity, its high catalytic activity for the hydrogen oxidation reaction (HOR) on the two phase boundaries (gas/Ceria) and its robustness against degradation.
Ceria based anodes are widely studied with thin-film symmetric cell setup, but less rigorously for the case of porous high-performance electrodes. Nevertheless, Ceria-based anodes are now at the threshold of commercialization. The requirements of the market call for higher performance and efficiency, longer lifetime and lower system costs. In this context a detailed understanding of the processes involved in Ceria-based porous high performance anodes on button cell, large area cell and stack levels is crucial in order to perform a systematic evaluation and optimization of the corresponding cell concepts and materials systems.

In SOFC research, electrochemical impedance spectroscopy (EIS) is an essential characterization tool, which serves as a basis for materials optimization on the electrode, cell and stack levels. However, for CGO based electrodes, there is no consensus how to interpret the impedance spectra yet. With EIS, the response from different processes in CGO based anodes are often not distinguishable from each other because their frequency ranges overlap and because of their interdependencies. Especially, on button cell level, it is often unclear which EIS-signals originate from chemical capacitance, surface reaction resistance, gas diffusion impedance and/or transport resistance.

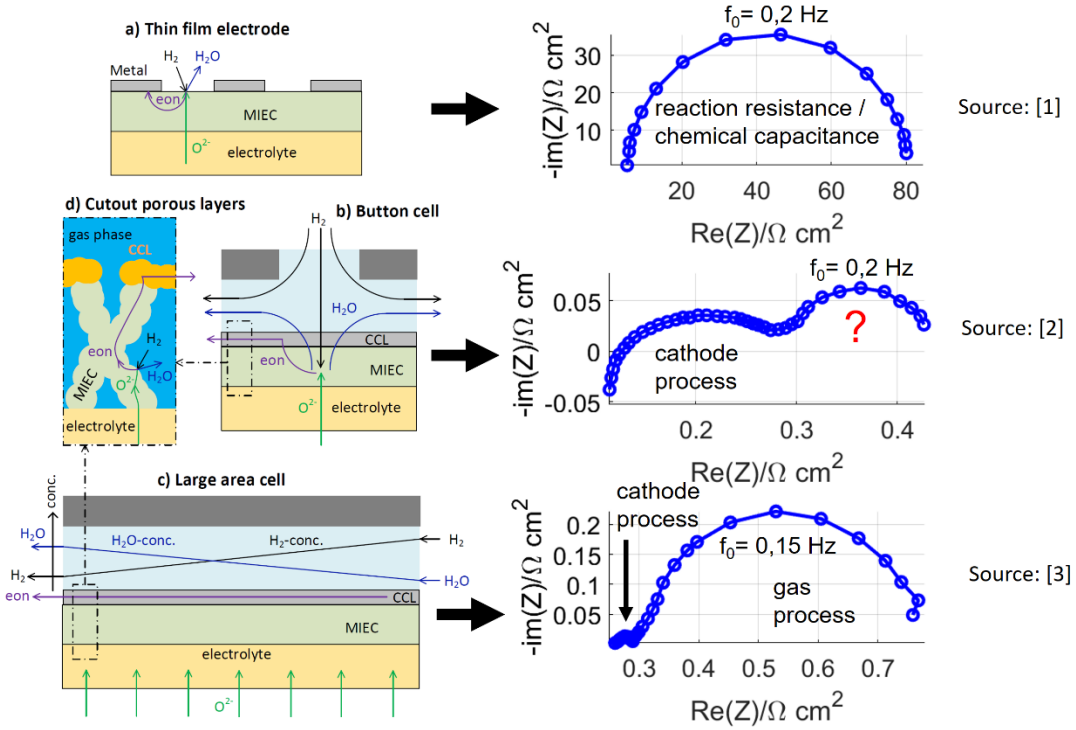

Figure 1: Illustration of the EIS-processes of Ceria-based electrodes on different levels, showing typical impedance spectra: a) from an SDC thin-film electrode (symmetric anode cell) showing a clear dominance of the chemical capacitance / surface reaction process, b) from a button cell (full cell with porous electrodes) with a CGO based anode, showing a low frequency process with non-obvious contributions from different processes and c) from a short stack consisting of large area full cells with CGO based anodes showing a clear dominance of the gas impedance process for the low frequency arc.

https://doi.org/10.5281/zenodo.4556899

In fact, there are some pitfalls when trying to link the impedance spectra of thin-film electrodes with those from porous high-performance electrodes. It is well accepted (e.g. [1], [4], [5]), that ceria based electrodes own a chemical capacitance, describing their ability to store energy by a change in stoichiometry. For ceria based thin film electrodes, other effects like the gas impedance and transport resistance of the charge carrier are negligible, and therefore the low-frequency arc can be attributed unequivocally to the chemical capacitance, which is linked with the electrochemical surface reaction (HOR) process. This mechanism is illustrated in Fig. 1 a), replotted from Chueh et al. [1]. On the other hand, for large area cells, the low frequency arc is clearly identified as a gas impedance process, because of the large gas conversion impedance due to the fuel consumption along the cell, as shown for a Hexis short stack in Fig. 1 c) with a CGO-Ni anode from Linder et al. [3]. In this case it is assumed that the (low frequency) contribution from chemical capacitance is relatively small and therefore hidden within the dominant gas impedance arc. In a button-cell setup with an excess fuel flow rate, the gas impedance is much smaller. In Fig. 1 b), a typical impedance spectrum for a button cell with a CGO based anode is shown from Riegraf et al. [2]. Whether this low frequency process in this case is dominated by the gas impedance, chemical capacitance / surface reaction process or even by a different process like the transport resistance of the charge carriers, is neither obvious nor trivial and different interpretations are found in the literature ([6], [7], [8], [9]).
In the present contribution, we will use a combined approach involving characterization methods like EIS and microstructure analysis as well as a simulation model to elucidate the contributions from gas impedance, chemical capacitance and surface reaction resistance and their interdependencies for button cell conditions.
A precise understanding and quantization of all the important physico-chemical processes involved is the basis for a systematic materials optimization of CGO-based anodes.

2. Approach for a systematic materials optimization of MIEC anodes

In Fig. 2, our approach for a systematic materials optimization of MIEC SOFC-electrodes is shown schematically.

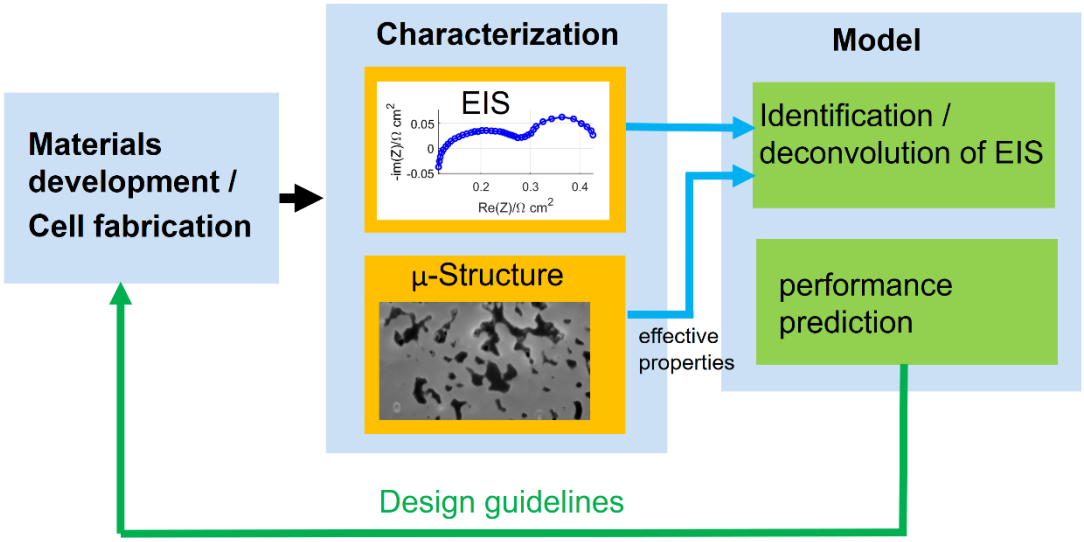

Figure 2: Approach for a systematic optimization of MIEC SOFC anodes with Materials development and cell fabrication on the button cell level (left), EIS characterization and quantitative 3D-microstructure analysis and determination of effective transport properties (centre), model for the deconvolution of EIS and identification of underlying (rate-limiting) processes and prediction of performance as a function of microstructure, operating conditions, cell architecture/layer thickness (right).

https://doi.org/10.5281/zenodo.4556899

The starting point for our systematic materials optimization approach is a batch of button-cells, which are fabricated based on detailed experimental know how at Hexis laboratories. The cell performance is characterized with electrochemical impedance spectroscopy (EIS). However, overlapping processes in the EIS spectra and lacking knowledge about the detailed physico-chemical processes makes it difficult to interpret the EIS-spectra correctly. Multi-physics simulation with AC and DC modes, enable the simulation of the EIS-spectra as well as the DC behavior during the normal cell operation. An essential prerequisite for an appropriate model is the knowledge about the effective properties of the microstructure. Microstructure analysis based on FIB-tomography enables to quantify morphological characteristics (tortuosity, porosity etc) and the associated transport properties. For details we refer to previous publications (e.g. Holzer et al. [17,18], Pecho et al [19], Neumann et al. [20,21], Stenzel et al.[22]).
Moreover, literature data for the bulk material properties is used in order to minimize the number of fit parameters. As illustrated below, this combination of characterization and modeling provides a basic understanding of the complex physico-chemical processes and enables the reliable deconvolution of EIS-spectra from fuel cells with ceria-based anodes.
The calibrated simulation model is then used to predict the impact of design adjustments (e.g. cell architecture, material and microstructure variations) on the cell performance. A key point thereby is to include the effects from the microstructure appropriately in the model. With the digital materials design (DMD) approach, the effect of microstructure variation on the cell performance can be assessed by generating virtual but realistic microstructures. By establishing the relation between material properties, microstructure, cell-design and performance, guidelines for a new anode materials design can be deduced. This allows for a faster and more systematic development of new SOFC electrodes. The different steps of the suggested approach are described in the following.

2.1 Cell fabrication and testing

The button-cells are fabricated by screen printing the anode and the cathode layers onto a 160 µm thick electrolyte disk from 6ScSZ (HEXIS). Both, the CGO and Nickel based anode layer and the double layered LSM/8YSZ and LSM cathode were prepared using the previously reported preparatory methods ([6],[10],[11]). The anode side is contacted with a Ni-mesh and the cathode side with a gold-mesh. The button-cells are operated on a seal-less button-cell test ridge at the laboratories of Hexis with a post-cell combustion zone. A more detailed description of the test ridge can be found in the work of Price et al. [6]. An excess hydrogen fuel supply on the anode side and an excess compressed air supply on the cathode side are used in order to avoid gas conversion impedance effects. The OCV and therewith the water content are varied by changing the fuel flow rate, which results in a specific gas composition due to the leakage of the seal-less setup. For the EIS-measurements a Zennium PP241 from Zahner is used.

2.2 Microstructure analysis

3D reconstructions of the microstructures from anodes are obtained by performing serial-sectioning with focused-ion beam scanning electron microscopy (FIB-SEM). The image size of each cross-section is about 13x9 µm with a (x-y) pixel resolution and (z-) slicing distance of 5 nm (Fig. 3). The 3D image is then segmented using GeoDict software (www.geodict.com). By means of image analysis and numerical simulations, metrics like the porosity and specific surface area and the transport properties for the gas and solid phase were determined using GeoDict. Because of the fine porous microstructure Knudsen and bulk diffusion are both relevant. The effective properties of a characteristic anode microstructure are summarized in Tab. 1 and will be discussed in more detail in the results

section. For details about the microstructure property relationships, we refer to previous publications (e.g. Holzer et al. [17,18], Pecho et al [19], Neumann et al. [20,21], Stenzel et al.[22]).

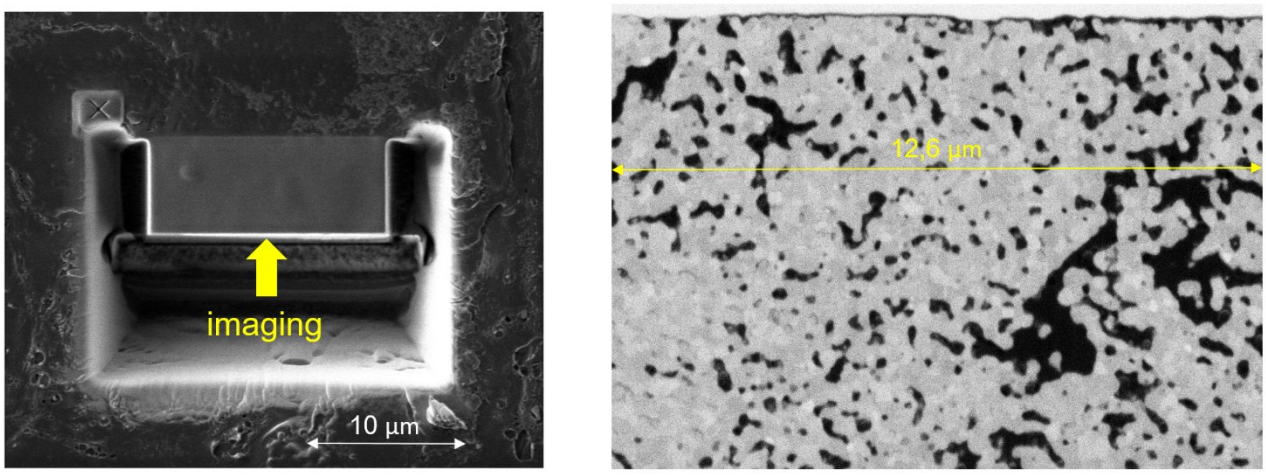

Figure 3: 3D imaging with FIB-tomography. a) Preparation of a cube for serial sectioning (top view, x-z-directions), b) SEM-cross-section with a voxel resolution of 5 nm (x-y).

2.3 Simulation model

For the simulation study, a 1D computational model is developed using the commercial software package Comsol Multiphysics [12]. The model consists of two computational domains as visualized schematically in Fig. 4.

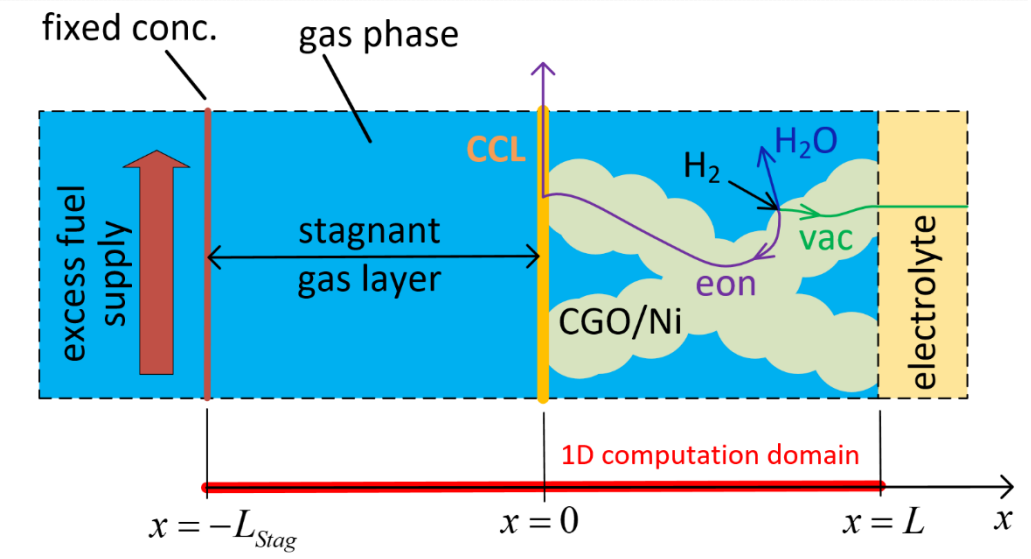

Figure 4: Illustration of the 1D simulation setup: eon = electrons, vac = oxygen ion vacancies, L_{Stag} = stagnant gas layer thickness, L = thickness of the porous CGO/Ni layer.

The domain from x = [0,L] is the porous CGO/Ni layer. It describes the transport of negatively charged Ce^{3+} ions (hereafter simply called electrons) and positively charged oxygen ion vacancies in the mixed ionic and electronic conductor (MIEC) CGO by drift and diffusion. Transport of gas species in the porous medium is described by a dusty gas model [13], which accounts for bulk and Knudsen diffusion. The hydrogen oxidation reaction (HOR) takes place at the CGO/pore interface, which is modelled as a source term as a consequence of the 1D setup.

The large volumetric chemical capacitance is a characteristic feature of (Ceria-based) MIEC-electrodes, which is associated by the storage of charges and a change of stoichiometry. The size of the chemical capacitance depends on the number of charge carriers. The number of charge carriers is a function of oxygen partial pressure and temperature and is implemented in the model according to experimental measurements from Wang et al. [14]. Also the ionic and electronic conductivities of CGO10 are implemented into the simulation model from Steele [15].
Based on the experimental setup, an excess fuel supply is assumed, resulting in a fixed gas species concentration at x = $-L_{Stag}$, avoiding any gas conversion impedance effect. Despite the excess fuel supply, there exists a stagnant gas layer above the electrode, where the gas transport is governed by diffusion and not by convection of the excess fuel supply. In the domain from x = [$-L_{Stag}$,0], the gas species diffusion in a stagnant gas layer is thus modelled. For the combined effect of the diffusion in the stagnant gas layer and in the porous CGO/Ni electrode the term gas diffusion impedance is used.
The electrolyte at x = L and the current collector layer at x=0 are only modelled as boundary conditions and are not spatially resolved. This model is described in great detail in a separate publication in preparation (P. Marmet et al., to be submitted to PCCP (Physical Chemistry Chemical Physics), Royal Society of Chemistry).

3. Results

3.1 EIS-Results

The Nyquist-plot of the EIS-spectra from a button-cell measured at T=850°C operated with a current density of J = 0.2 A/cm^2 is shown in Fig. 5. The water content was calculated from the OCV to be x_{H2O} = 0.0844. The anode processes and the cathode-processes can be clearly distinguished. However, for the current study we are only intersted in the anode processes.

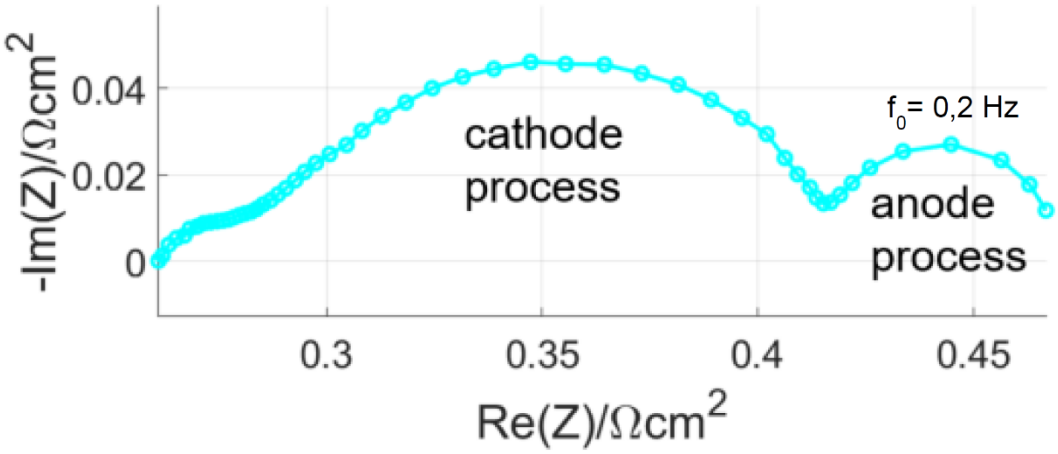

Figure 5: Nyquist-plot of the EIS-spectra measured at T=850°C, current density J = 0.2 A/cm^2 and a water content of x_{H2O} = 0.0844.

As mentioned in the introduction, the anode contributions to the EIS-spectra appear as only one single LF-arc and the different contributions can not be distinguished, which hinders a systematic optimization. Therefore, a physical model is needed to deconvolute these processes.

https://doi.org/10.5281/zenodo.4556899

3.2 Microstructure and effective properties

A crucial prerequisite for appropriate simulation results is the knowledge of the effective transport properties and other microstructure metrics, which are summarized in table 1. The CGO-Ni layer thickness was estimated to 20 µm, but was difficult to measure precisely because of a considerable variation of the thickness along the cell. The sample is quite dense and shows a porosity of ε = 0.213. The hydrogen oxidation reaction (HOR) scales proportionally with the surface of the CGO/gas interface. Because of the low porosity, the relative bulk gas diffusivity and the gas permeability are quite low (note: the relative properties are subsequently also named as microstructure factor, defined as M = (effective porous material property)/(bulk material property)). The characteristic pore diameter is about 125 nm and therewith, Knudsen diffusion is relevant and is even the dominant diffusion resistance as the effective Knudsen numbers for hydrogen and water are larger than one. The relative Knudsen diffusivity, which is determined by a random walk algorithm, is in the same order of magnitude but not identical to the relative bulk diffusivity, which is determined by solving the diffusion equation on the voxel mesh. All these effective properties for the pore phase enter into the dusty gas model, which describes the combined effects of bulk and Knudsen diffusion appropriately. Because of the high solid volume fraction, the relative electric conductivity is quite high. Using these effective properties, the effect of the microstructure can be captured reliably in the simulation model. However, an uncertainty of such an effective property model enters by the fact, that the CGO/Ni layer contains local cracks (not shown), which cross-cut the entire anode layer. As these cracks are not yet respected in the current model description, the transport resistance in the pore phase tends to be overestimated while the transport resistance in the solid phase tends to be underestimated.

CGO/Ni Layer Thickness / µm	20
Porosity (Epsilon) / -	0.213
Specific Surface Area (S) / μm^{-1}	4.29
Relative Bulk Gas Diffusivity (D_rel_sim) / -	0.0163
Gas Permeability (Kappa_sim) / m^2	9.79E-17
Characteristic pore diameter / nm	125.31
Relative Knudsen Diffusivity	0.0122
Effective Knudsen number Kn for H2	6.39
Effective Knudsen number Kn for H2O	4.86
Solid Volume Fraction (Phi) / -	0.787
Relative Electric Conductivity (Sigma_rel_sim) / -	0.623

Tabel 1: Summary of microstructure characteristics and effective properties.

3.3 Simulation results

The microstructure properties enter into the simulation model together with bulk material properties from literature. The only fit parameter in the model is the exchange reaction rate for the HOR, which is very hard to determine appropriately in an analytical way or from literature. This now allows for a deconvolution of the EIS-spectrum into the different contributions from distinct anode processes. The simulation results are plotted along with the experimental EIS-measurements in Fig. 6. The Nyquist-plot in Fig. 6 a) shows that the surface reaction resistance Z_{SR} of the HOR has the largest contribution from all anode processes (note: the surface reaction resistance is strongly linked with the chemical capacitance). The gas diffusion impedance Z_{gas} contributes also substantially to the anode

arc (due to low porosity and small pore size associated with the dense anode microstructure), while the resistance for the transport of the charge carriers $Z_{transport}$ is negligible for an anode with such a dense microstructure and relatively small CGO/Ni layer thickness.
The imaginary part of the impedance in Fig. 6 b) also shows a good agreement between simulation and EIS-measurement in the low frequency range. This result points out that the computed chemical capacitance is in a reasonable range. It must be emphasized that the chemical capacitance is not fitted, but instead it is determined directly with the model. Thereby, the result for chemical capacitance (and Z_{SR}, respectively) strongly depends on the charge carrier concentration, which is implemented from literature data.

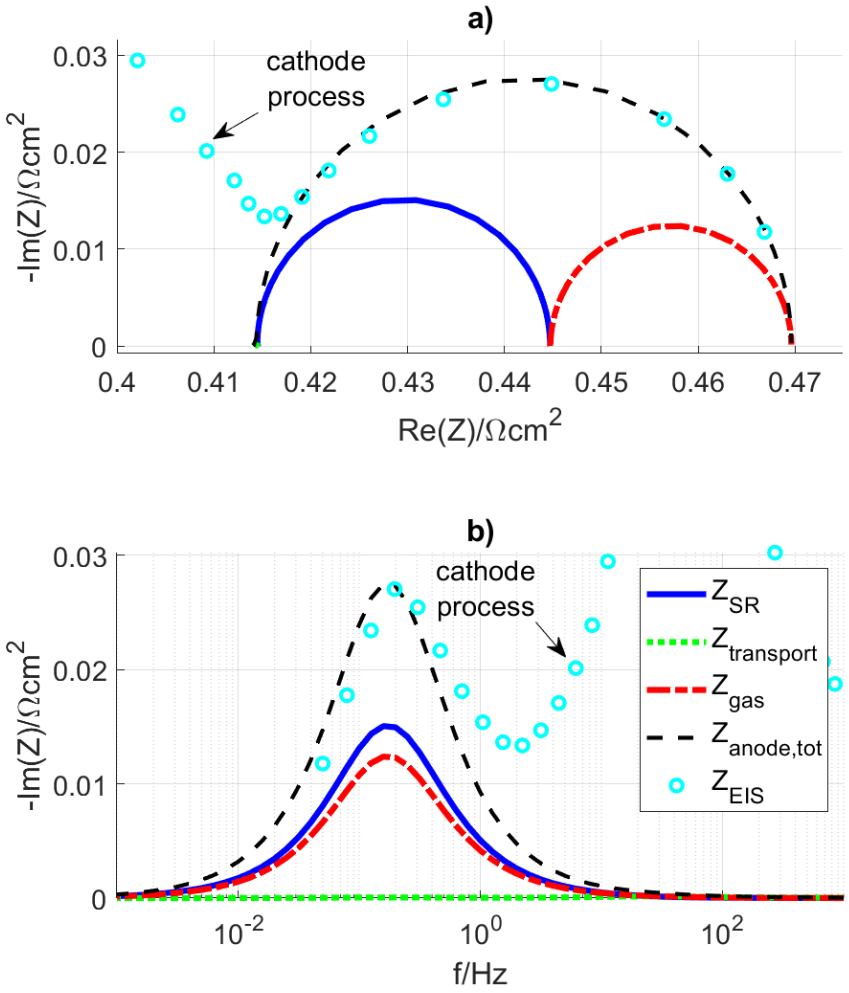

Figure 6: Simulation-based deconvolution of process-related contributions to the anode impedance spectrum and comparison with experimental data (Z_{EIS}). a) Nyquist impedance plot and b) imaginary part of the impedance for the surface reaction impedance Z_{SR}, impedance associated with the charge carrier transport in the CGO layer $Z_{transport}$, gas diffusion impedance Z_{gas}, total anode impedance $Z_{anode,\,tot}$ and experimental data (Z_{EIS}).
Moreover, the simulation shows, that the gas impedance Z_{gas} and the surface reaction impedance Z_{SR} have exactly the same characteristic frequency! This is not by chance, but a consequence of the way these two processes are coupled. An RC-like arc in an impedance spectra results always in bypassing the resistance by just oscillating the charge in the capacitor. For the surface reaction impedance that means, that the surface reaction resistance is bypassed and that there is no change in the surface reaction due to the applied perturbation at all, because the harmonic current is entirely stored in the chemical capacitance! And if there is no effect on the reaction anymore, there is also no effect on the gas concentration at the electrode surface. And if the concentration does not

change anymore, also the gas impedance is bypassed. Due to this strong coupling, the gas impedance process is forced to the same frequency as the surface reaction process and the two processes cannot be distinguished experimentally in an EIS-spectra of a button cell! The situation might be different for large area cells and stacks. Here, the anode arc is usually dominated by the gas impedance. If the characteristic frequency of the gas impedance is lower than the surface reaction / chemical capacitance impedance process, the two processes are theoretically distinguishable from each other.
Even if this deconvolution of distinct anode processes might appear as a detail for the overall cell performance, it is crucial for a systematic optimization of the anode electrode! If e.g. the anode ASR shall be optimized for a cell where the largest contribution is the surface reaction resistance, the layer thickness can be increased or the fabrication process can be tailored to a microstructure with higher active surface area, which then lowers the surface reaction resistance. At the same time the gas impedance may increase as a trade-off. For a cell, where the gas impedance represents the dominant contribution to the anode arc, the opposite measure (i.e. thinner and less dense anode) potentially leads to an improvement of the total anode performance. This example illustrates, that a systematic optimization is only possible with a detailed understanding of the relevant physico-chemical processes involved.

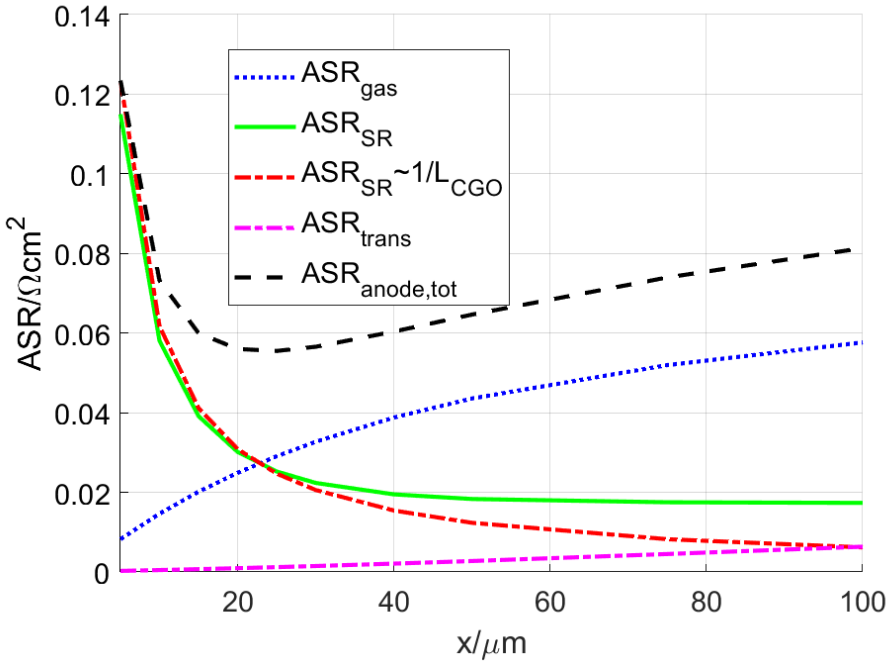

Figure 7: Simulation results of the different contributions to the total anode area specific resistance (ASR) as a function of the CGO/Ni layer thicknesses assuming identical microstructures for all thicknesses. ASR_{SR}: surface reaction resistance, ASR_{trans}: resistance associated with the charge carrier transport in the CGO/Ni layer, ASR_{gas}: gas diffusion resistance and $ASR_{anode,\ tot}$: total anode area specific resistance.

As a simple example for model based-optimization, the thickness of the CGO/Ni layer is changed continuously. Thereby, it is assumed that the operating conditions and microstructure properties remain identical for all thicknesses. The different contributions to the anode ASR extracted from AC simulations are shown in Fig. 7. The optimal thickness for the specific operating conditions and microstructure is about 25 µm. For smaller thicknesses, the total anode ASR rises steeply, because the active surface for the HOR reaction becomes too small. For thicknesses larger than 25 µm, the total ASR anode increases, but with a shallower slope. As a rule of thumb it is often assumed that ASR_{tot} with a minimum is due the two following thickness effects: the gas impedance ASR_{gas}

increases linearly with the thickness, and the surface reaction impedance ASR_{SR} decreases inverse proportional to the thickness (1/L). Our model calculations show that these rules are not precise:
The contribution of the gas impedance ASR_{gas} does not increase linearly but sub-proportional with the layer thickness. In addition, the contribution of the surface reaction impedance ASR_{SR} decreases less than inverse proportional to the layer thickness (the inverse proportional line is plotted as a reference in Fig. 7). This behaviour can be easily understood by considering the DC-result from the extension of the reaction zone in Fig. 8.

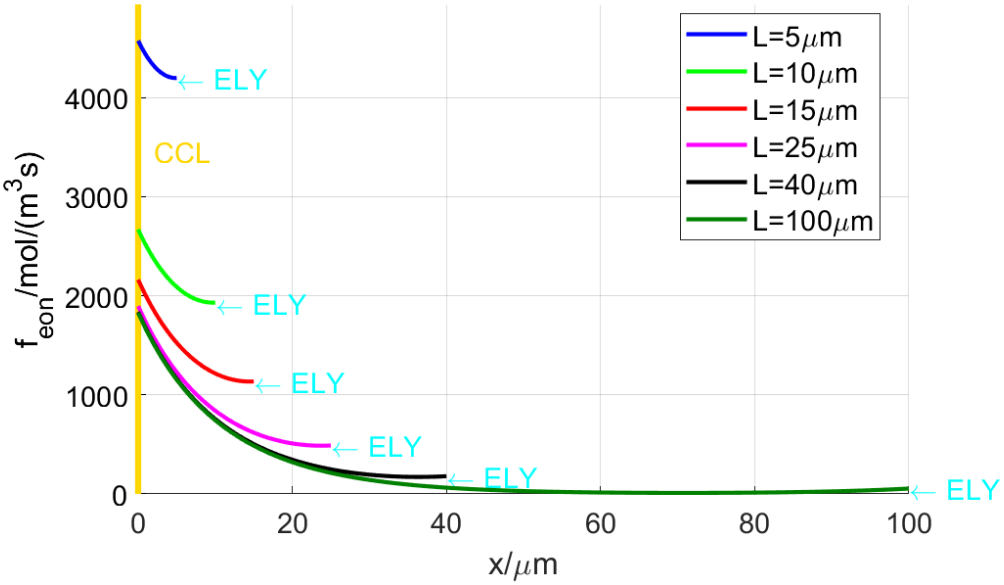

Figure 8: Surface reaction rate (source term of electrons) across the CGO/Ni layer for different CGO/Ni layer thicknesses.

For small CGO/Ni layer thicknesses (e.g. L = 5 µm) high reaction rate is distributed almost homogeneously over the entire CGO/Ni layer. For larger CGO/Ni layer thicknesses, the reaction zone (i.e. domain with high reaction rate) is concentrated close to the CCL in order to minimize the pathways for gas transport in the very dense microstructure. Hence, in thick anodes only a relatively small part of the CGO/Ni layer is electrochemically active and the surface reaction resistance only decreases slightly with increasing layer thickness. At the same time, the increase of the gas impedance with growing thickness is limited, as the gas species only have to be transported to the active zone. Note, that for higher porous microstructures, where the charge transport impedance is larger than the gas diffusion impedance, the reaction zone would be shifted towards the interface with the electrolyte in order to minimize the losses from charge transport (not shown here).

https://doi.org/10.5281/zenodo.4556899

3.4 Influence of the operating conditions

In order to ensure a robust materials design, the dependency of the anode resistance on the operating conditions is investigated in a combined experimental/modeling approach. As shown in Fig. 9, the total ASR anode $ASR_{tot,exp}$ is fitted for experimental EIS-data for different water fractions at OCV. A large variation of about a factor of 3 can be observed, demonstrating the importance of paying attention to the dependency on operating conditions. The total anode $ASR_{tot,exp}$ essentially deconvolutes in a contribution of the surface reaction resistance / chemical capacitance process and the gas diffusion impedance process. The gas diffusion resistance ASR_{gas} can be calculated from the model and the results is plotted in Fig. 9. As mentioned before, the surface reaction resistance is difficult to be determined analytically and precise experimental characterizations describing the impact of gas composition (water content) are not available. Therefore, we estimate the dependency of the surface reaction resistance $ASR_{SR,estimated}$ as the difference between the experimentally measured total ASR of the anode $ASR_{tot,exp}$ and the simulated gas diffusion resistance ASR_{gas}, neglecting other contributions as e.g. the resistance from charge carrier transport. The result $ASR_{SR,estimated}$ is plotted in Fig. 9.
From literature it is known, that the surface reaction resistance depends on the oxygen partial pressure p_{O2} and water content x_{H2O} (e.g. [2,16]). Therefore, an expression for the surface reaction resistance as a function of p_{O2} and x_{H2O} shall be suggested. For the present case of humid hydrogen, the oxygen partial pressure varies according to the dissociation of water according the following law:

$$p_{O_2} = \left(\frac{p_{H_2O}}{p_{H_2}} \right)^2 \frac{1}{K_p} \quad \text{(Equation 1)}$$

where K_p is the equilibrium constant of the reaction. Therewith, we a have a relationship between p_{O2} and x_{H2O} available.

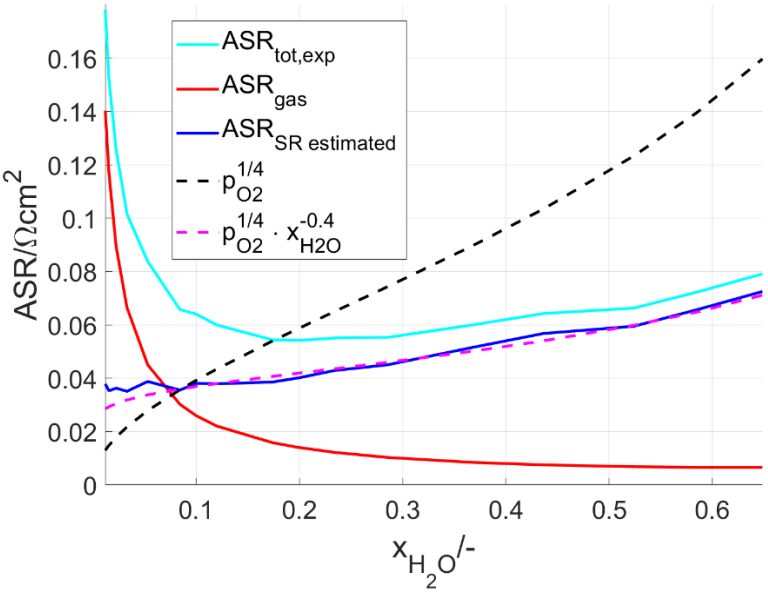

Figure 9: Dependency of the anode ASR on the water fraction at OCV. $ASR_{tot,exp}$: total anode ASR from experimental EIS-measurements extracted by circuit fitting, ASR_{gas}: simulated gas diffusion resistance, $ASR_{SR\ estimated}$: estimated surface reaction resistance calculated as $ASR_{SR\ estimated} = ASR_{tot,exp} - ASR_{gas}$, black dashed line: $p_{O2}^{1/4}$-law as reference, magenta dashed line: $p_{O2}^{1/4}\ x_{H2O}^{-0.4}$-law as reference.

https://doi.org/10.5281/zenodo.4556899

As a reference, the $p_{O2}^{1/4}$-law, which is often reported as a dependency on the oxygen partial pressure of the surface reaction resistance of Ceria-based electrodes (e.g. Chueh et al. [16]), is plotted as black dashed line with x_{H2O} = 0.0844 as a reference point, which has been used for the study above. The oxygen partial pressure p_{O2} is thereby calculated from the water content according to equation 1. The curve of the $p_{O2}^{1/4}$-law is much steeper than the estimated curve for the surface reaction resistance that is fitted for varying p_{H2O}. This is in accordance with the observation of e.g. Riegraf et al. [2] according to whom the water concentration reduces the surface reaction resistance and therefore possibly acts as a catalyst for the HOR. A reasonable agreement for the current data set can be achieved by using a power law for the water fraction dependency with an exponent of approximately -0.4 (see the magenta dashed line with the $p_{O2}^{1/4}$ $x_{H2O}^{-0.4}$-law). In this way, the surface reaction resistance can be calibrated as a function of the water content based on a fitting-procedure with EIS-measurements.

4. Summary and Outlook

We present an approach for a systemtic materials optimization for CGO-based anodes including EIS-measurments, microstructure characterization and simulation models. The EIS-measurements and the effective properties of the microstructure can be used to achieve an appropriate simulation model, which is able to capture all relevant physico-chemical processes involved and to extract valuable information for the optimization of the electrode, which are blurred in the experimental impedance spectra. We especially point out, that the anode arc for button cell conditions often includes a gas diffusion impedance and a surface reaction resistance / chemical capacitance process, which are not distinguisable experimentally. The correct interpretation of the EIS-spectra with identification of the dominant, rate limitting process is only possible in combination with an appropriate model. For the situation of thin film electrodes, the surface reaction resistance / chemical capacitance process (Fig. 1 a)) and for large area cells, the gas impedance process (Fig. 1 c)) are typically dominant. We also show that the operating conditions have a large impact on the cell performance. EIS-measurements at different water contents show, that the total anode ASR changes about a factor of 3 as a function of the water content. We also present an approach to describe quantitatively the dependency on the water content of the different contributions of gas impedance and surface reaction resistance.

The knowledge about a) the relevant physico-chemical processes, b) the associated material laws and microstructure effects and c) the dependencies on varying operating conditions is a crucial prerequisite for a systemic materials optimization. If all those aspects are implemented in a comprehensive simulation model, the optimization process can be performed in a very efficient way, as it has been exemplarily shown for the optimization of the CGO/Ni layer thickness assuming a constant microstructure.

As an outlook, the full potential of the suggested model approach can be exploited in combination with the digital materials design (DMD) approach using virtual microstructures. Thereby, a stochastic digital twin of a reference microstructure from FIB-SEM imaging is deduced, which allows for a virtual but realistic variation of the microstructure. The effect of the microstructure variation on the cell performance can be assessed by the simulation model (virtual materials testing, VMT). Based on a set of experimental data this approach enables a fully digital materials optimization providing design guidelines for the next experimental steps, allowing for a faster and more systematic optimization of the next generation of MIEC-based anodes.

https://doi.org/10.5281/zenodo.4556899

References

[1] W. C. Chueh and S. M. Haile, “Electrochemical studies of capacitance in cerium oxide thin films and its relationship to anionic and electronic defect densities,” Phys. Chem. Chem. Phys., vol. 11, no. 37, pp. 8144–8148, 2009

[2] M. Riegraf, V. Yurkiv, R. Costa, G. Schiller, and K. A. Friedrich, “Evaluation of the Effect of Sulfur on the Performance of Nickel/Gadolinium-Doped Ceria Based Solid Oxide Fuel Cell Anodes,” ChemSusChem, vol. 10, no. 3, pp. 587–599, 2017.

[3] M. Linder et al., “A model-based approach for current voltage analyses to quantify degradation and fuel distribution in solid oxide fuel cell stacks,” J. Power Sources, vol. 288, pp. 409–418, 2015.

[4] J. Jamnik and J. Maier, “Treatment of the impedance of mixed conductors. Equivalent circuit model and explicit approximate solutions,” J. Electrochem. Soc., 1999.

[5] W. Lai and S. M. Haile, “Impedance spectroscopy as a tool for chemical and electrochemical analysis of mixed conductors: A case study of ceria,” J. Am. Ceram. Soc., vol. 88, no. 11, pp. 2979–2997, 2005.

[6] R. Price, M. Cassidy, J. G. Grolig, A. Mai, and J. T. S. Irvine, “ Preparation and Testing of Metal/Ce 0.80 Gd 0.20 O 1.90 (Metal: Ni, Pd, Pt, Rh, Ru) Co-Impregnated La 0.20 Sr 0.25 Ca 0.45 TiO 3 Anode Microstructures for Solid Oxide Fuel Cells ,” J. Electrochem. Soc., vol. 166, no. 4, pp. F343–F349, 2019.

[7] S. Primdahl and M. Mogensen, “Mixed conductor anodes: Ni as electrocatalyst for hydrogen conversion,” Solid State Ionics, vol. 152–153, pp. 597–608, 2002.

[8] P. V. Aravind, J. P. Ouweltjes, and J. Schoonman, “Diffusion impedance on nickel/gadolinia-doped ceria anodes for solid oxide fuel cells,” J. Electrochem. Soc., vol. 156, no. 12, 2009.

[9] T. Nakamura et al., “Determination of the Reaction Zone in Gadolinia-Doped Ceria Anode for Solid Oxide Fuel Cell,” J. Electrochem. Soc., 2008. [4] J. Jamnik and J. Maier, “Treatment of the impedance of mixed conductors. Equivalent circuit model and explicit approximate solutions,” J. Electrochem. Soc., 1999.

[10] R. Price et al., “Development and Testing of Impregnated $La_{0.20}Sr_{0.25}Ca_{0.45}TiO_3$ Anode Microstructures for Solid Oxide Fuel Cells“, ECS Trans., 78(1),1385 (2017).

[11] R. Price et al., “Screen Printed Porous $La_{0.20}Sr_{0.25}Ca_{0.45}TiO_3$ Fuel Electrode Scaffold Microstructures: Optimisation of Interaction with Impregnated Catalysts for More Durable Performance “, ECS Trans., 68(1), 1499 (2015).

[12] COMSOL Multiphysics® v. 5.5. www.comsol.com. COMSOL AB, Stockholm, Sweden.

[13] S. Liu, W. Kong, and Z. Lin, “Three-dimensional modeling of planar solid oxide fuel cells and the rib design optimization,” J. Power Sources, vol. 194, no. 2, pp. 854–863, 2009.

[14] S. WANG, H. INABA, H. TAGAWA, M. DOKIYA, and T. HASHIMOTO, “Nonstoichiometry of Ce 0. 9 Gd 0. 1 O 1. 95-x,” Solid state ionics, 1998.

[15] B. C. H. Steele, “Appraisal of Ce1-yGdyO2-y/2 electrolytes for IT-SOFC operation at 500,” Solid State Ionics, vol. 129, no. 1, pp. 95–110, 2000.

[16] W. C. Chueh, W. Lai, and S. M. Haile, “Electrochemical behavior of ceria with selected metal electrodes,” Solid State Ionics, vol. 179, no. 21–26, pp. 1036–1041, 2008.

[17] L. Holzer, B. Münch, B. Iwanschitz, M. Cantoni, T. Hocker, T. Graule, Quantitative relationships between composition, particle size, triple phase boundary length and surface area in nickel-cermet anodes for Solid Oxide Fuel Cells, J. Power Sources. 196 (2011) 7076–7089. doi:10.1016/j.jpowsour.2010.08.006.

[18] L. Holzer, B. Iwanschitz, T. Hocker, L. Keller, O. Pecho, G. Sartoris, et al., Redox cycling of Ni–YSZ anodes for solid oxide fuel cells: Influence of tortuosity, constriction and percolation factors on the effective transport properties, J. Power Sources. 242 (2013) 179–194. doi:10.1016/j.jpowsour.2013.05.047.
[19] O. Pecho, O. Stenzel, B. Iwanschitz, P. Gasser, M. Neumann, V. Schmidt, et al., 3D Microstructure Effects in Ni-YSZ Anodes: Prediction of Effective Transport Properties and Optimization of Redox Stability, Materials (Basel). 8 (2015) 5554–5585. doi:10.3390/ma8095265.
[20] M. Neumann, O. Stenzel, F. Willot, L. Holzer, V. Schmidt, Quantifying the influence of microstructure on effective conductivity and permeability: Virtual materials testing, Int. J. Solids Struct. 184 (2020) 211–220. doi:10.1016/j.ijsolstr.2019.03.028.
[21] M. Neumann, O. Furat, D. Hlushkou, U. Tallarek, L. Holzer, V. Schmidt, On Microstructure-Property Relationships Derived by Virtual Materials Testing with an Emphasis on Effective Conductivity, in: Sim Sci, Commun. Comput. Inf. Sci., 2018: pp. 145–158. doi:10.1007/978-3-319-96271-9_9.
[22] O. Stenzel, O. Pecho, L. Holzer, M. Neumann, V. Schmidt, Big data for microstructure-property relationships: A case study of predicting effective conductivities, AIChE J. 63 (2017) 4224–4232. doi:10.1002/aic.15757.

Keywords: EFCF2020, SOx
Session A15: Cell, stack & system modelling and optimization
Remark: This work is licensed under Creative Commons Attribution 4.0 International